Measurements of a Barotropic Planetary Vorticity Mode in an Eddy-Resolving Quasi-Geostrophic Model Using Acoustic Tomography

by

Wendy B. Lawrence

B.S. Ocean Engineering, United States Naval Academy (1981)

Submitted in partial fulfillment of the
requirements for the degree of

MASTER OF SCIENCE IN OCEAN ENGINEERING

at the

MASSACHUSETTS INSTITUTE OF TECHNOLOGY

and the

WOODS HOLE OCEANOGRAPHIC INSTITUTION

August 1988

Signature of Author .....
Joint Program in Oceanographic Engineering
Massachusetts Institute of Technology
Woods Hole Oceanographic Institution
August 5, 1988

Certified by .....
Dr. John L. Spiesberger
Woods Hole Oceanographic Institution
Thesis Supervisor

Certified by .....
Dr. Arthur B. Baggeroer
Massachusetts Institute of Technology

Accepted by .....
Dr. W. Kendall Melville
Chairman, Joint Committee for Oceanographic Engineering
Massachusetts Institute of Technology/Woods Hole Oceanographic Institution

Measurements of a Barotropic Planetary Vorticity Mode in an Eddy-Resolving Quasi-Geostrophic Model Using Acoustic Tomography

by

Wendy B. Lawrence

Submitted to the Massachusetts Institute of Technology/
Woods Hole Oceanographic Institution
Joint Program in Oceanographic Engineering
on August 5, 1988, in partial fulfillment of the
requirements for the degree of
Master of Science in Ocean Engineering

Abstract

A tomographic array is placed in a 2-layer, flat bottom, steady-wind driven quasi-geostrophic circulation model to investigate whether the analysis of acoustic travel time changes can detect large-scale barotropic oscillations. Time series of sea surface elevation and upper and lower layer meridional currents are generated for comparison against a series of acoustic travel times. The spectra of these time series exhibit a broad mesoscale peak near a period of 40 days. The spectrum of the acoustic travel time contains a significant peak due to a resonant barotropic oscillation with a period of 28.6 days which is not present in the spectra of the point measurements. In this numerical model, basin-scale tomographic measurements are a better method of sensing the large-scale resonant barotropic oscillations than are conventional point measurements because the tomographic system attenuates the "noise" from the mesoscale.

Thesis Supervisor: Dr. John L. Spiesberger
Woods Hole Oceanographic Institution

Acknowledgements

I am extremely grateful to my thesis advisor, Dr. John Spiesberger, for his guidance. His knowledge, understanding and insight enabled the completion of this thesis.

I am also indebted to Dr. Arthur Miller for the use of his data from the QG model. His knowledge of the model's dynamics and timely suggestions greatly facilitated my research.

I would like to thank the United States Navy for the opportunity to pursue graduate education through the MIT/WHOI Joint Program. And now, this rotorhead is ready to have the terminals that I see be the ones located next to runways.

Special thanks go to Maxine Jones whose mastery in computer programming proved to be invaluable.

To my officemates, Liz and Raj, I would like to say that I am very grateful for your constant support and encouragement. I am glad that we went through this together.

I would like to express my deep appreciation to my roommate, Meg, for her unselfish enduring of my times on "det" and her endless sharing of the load.

Finally I thank God for daily giving me the strength, endurance, courage and insight to keep "plodding" along through the many ups and downs of this academic experience.

Contents

1 7

1.1 Introduction 7

1.2 The Forward Problem 8

1.3 The Forward Problem for Modes 11

1.4 Selection of Section Location 12

1.5 Spectral Analysis 15

1.6 Discussion 21

List of Figures

1 The vertical structure of the 2-layer, QG model 9

2 Climatological potential sound speed gradient in the Northeast Pacific . . . 11

3 Meridional section of sound speed in the Northeast Pacific 14

4 Instantaneous perturbation interface displacement of the QG model 16

5 Instantaneous streamfunction maps of the QG model 17

6 Time series of acoustic travel time change with detrending smoothed cubic spline 19

7 Time series of sea surface elevation, upper and lower layer meridional current and detrended acoustic travel time change 20

8 Power spectral densities of sea surface displacement, meridional currents and acoustic travel time change 22

9 Power spectral density of acoustic travel time change in the eddy field . . . 23

List of Tables

1 The scales of mode 17 in the QG model 15

2 The predicted and computed values of rms travel time change and power spectral density level 21

Chapter 1

1.1 Introduction

The resonant barotropic oscillations (modes) predicted by the quasi-geostrophic (QG) theory are difficult to observe in the ocean. Large-scale measurements over lengthy durations may be required in order to observe these waves. For example, Luther (1982) presents evidence from 2 to 7 years of sea level records from Pacific islands that suggests the presence of a 4 to 6 day barotropic planetary oscillation.

The capability of receiving long-range sound transmissions in the ocean implies that acoustic methods may be well-suited for the study of large-scale motions. In particular, basin-scale tomographic arrays may provide the coverage over sufficient time periods as well as the sensitivity needed to resolve the modes (Bushong, 1987 and Spiesberger et al., 1988a).

In this study, we investigate whether the analysis of the travel time fluctuations of tomographic transmissions can detect large-scale barotropic planetary oscillations in a QG model. We use four years of data from the 2-layer, steady-wind, flat bottom eddy-resolving general circulation model in which Miller (1986) detected barotropic modes. A tomographic array is placed in the model and a time series of travel time changes is computed. We compare this series against series of sea surface elevation and current to determine if acoustic tomography can provide an effective method of detecting barotropic modes.

Section 1.2 describes how tomographic travel times are influenced by fluctuations of the temperature, pressure and currents in a QG model. Section 1.3 describes the response of the acoustic travel times due to resonant barotropic oscillations. Section 1.4 describes the geometry and location of the tomographic section in the QG model. Section 1.5 presents results of the analysis of the tomographic, sea surface elevation, and current time series. A discussion follows in section 1.6.

1.2 The Forward Problem

A. Definitions

The change in the travel time along the acoustic ray path Γ_0 at geophysical time t is approximately given by,

$$\delta T(t) = -\int_{\Gamma_0} \frac{1}{c_0^2(z_{ray})}\left[\eta\frac{\partial c_p}{\partial z} + \gamma\delta p + \vec{u}\cdot\hat{s}\right]ds \quad , \tag{1.1}$$

where the reference sound speed profile is $c_0(z)$ and the increment of ray path is ds with unit vector $\hat{s}$. A Cartesian coordinate system is adapted where x is positive to the east with unit vector $\hat{\imath}$, y is positive to the north with unit vector $\hat{\jmath}$ and z is positive upwards with unit vector $\hat{k}$. Vectors are denoted by arrows.

The travel time is affected by three processes. One, the vertical displacement of water (positive up), $\eta(\vec{s},t)$, approximately changes the in-situ speed of sound by,

$$\delta c(\vec{s},t) \cong \eta(\vec{s},t)\frac{\partial c_p(\vec{s},t)}{\partial z} \quad , \tag{1.2}$$

where the potential sound speed is c_p (Munk et al., 1981). Two, changes in the hydrostatic pressure, $\delta p(\vec{s},t)$, which arise from surface displacements, alter the in-situ sound speed by,

$$\delta c(\vec{s},t) \cong \gamma\delta p(\vec{s},t) \quad , \tag{1.3}$$

where the proportionality constant, γ, is approximately 1.682×10^{-6} m s^{-1} Pa^{-1}

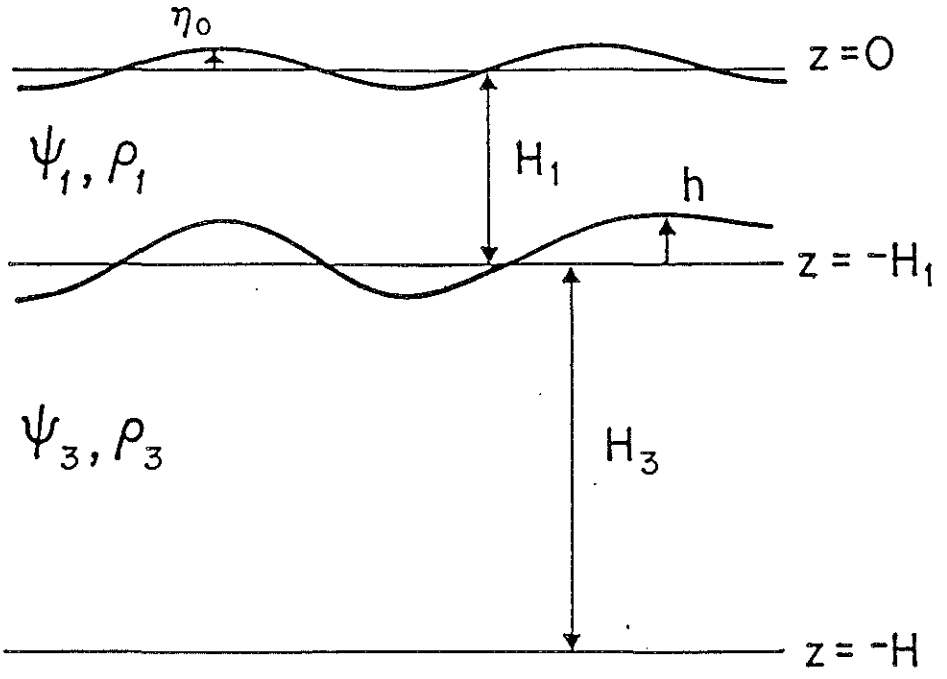

Fig. 1. Definition figure of the quantities computed in the quasi-geostrophic model. The undisturbed depth is H and the undisturbed layer thicknesses are H_1 (1000 m) and H_3 (4000 m). The interface displacement is h and the surface displacement is η_0 (both positive up). The streamfunction in the upper and lower layers is ψ_1 and ψ_3, respectively. The densities in the layers are ρ_1 and ρ_3.

(Munk, 1974). Three, the projection of the horizontal current,

$$\vec{u}(\vec{s},t) = u(\vec{s},t)\hat{\imath} + v(\vec{s},t)\hat{\jmath} \quad , \tag{1.4}$$

onto the unit vector, $\hat{s}$, along the ray path also affects the travel time. The position of a ray is given by,

$$\vec{s} = x_{ray}\hat{\imath} + y_{ray}\hat{\jmath} + z_{ray}\hat{k} \quad .$$

Vertical currents are negligible in this study.

B. Relation to the Quasi-Geostrophic Model

The quantities computed in the quasi-geostrophic model are shown in Figure 1. The

vertical water displacement is given by,

$$\eta(x,y,z,t) = \begin{cases} \frac{-h(x,y,t)z}{H_1} & z > -H_1 \quad \text{(upper layer)} \\ \frac{h(x,y,t)(H+z)}{H-H_1} & z \leq -H_1 \quad \text{(lower layer)} \end{cases} \quad . \tag{1.5}$$

The perturbation pressure is,

$$\delta p(x,y,z,t) = \begin{cases} \rho_0 f_0 \psi_1(x,y,t) & z > -H_1 \quad \text{(upper layer)} \\ \rho_0 g \eta_0(x,y,t) + \rho_0 g' h(x,y,t) & z \leq -H_1 \quad \text{(lower layer)} \end{cases} \quad , \tag{1.6}$$

where the mean density is ρ_0, the Coriolis parameter is f_0 and the reduced gravity is,

$$g' = \frac{g(\rho_3 - \rho_1)}{\rho_0} \quad .$$

The interface displacement is given by,

$$h(x,y,t) = (\frac{f_0}{g'})(\psi_1(x,y,t) - \psi_3(x,y,t)) \quad , \tag{1.7}$$

(Holland, 1978). The horizontal currents are given by,

$$\begin{aligned} u_i(x,y,t) &= -\frac{\partial \psi_i(x,y,t)}{\partial y} \quad (i = 1,3) \quad , \\ v_i(x,y,t) &= \frac{\partial \psi_i(x,y,t)}{\partial x} \quad (i = 1,3) \quad . \end{aligned} \tag{1.8}$$

Parameter values are $\rho_0 = 1025.0$ kg m^{-3}, $f_0 = 9.3 \times 10^{-5}$ s^{-1} and $g' = .02$ m s^{-2}. The origin of the coordinate system is the lower left hand corner of the model (Fig. 5).

The QG model does not include thermodynamics. Therefore, the potential sound speed gradient is taken from a climatological average in the Northeast Pacific (Fig. 2). The gradient is small below a depth of about one kilometer because the ocean is nearly adiabatic in this region.

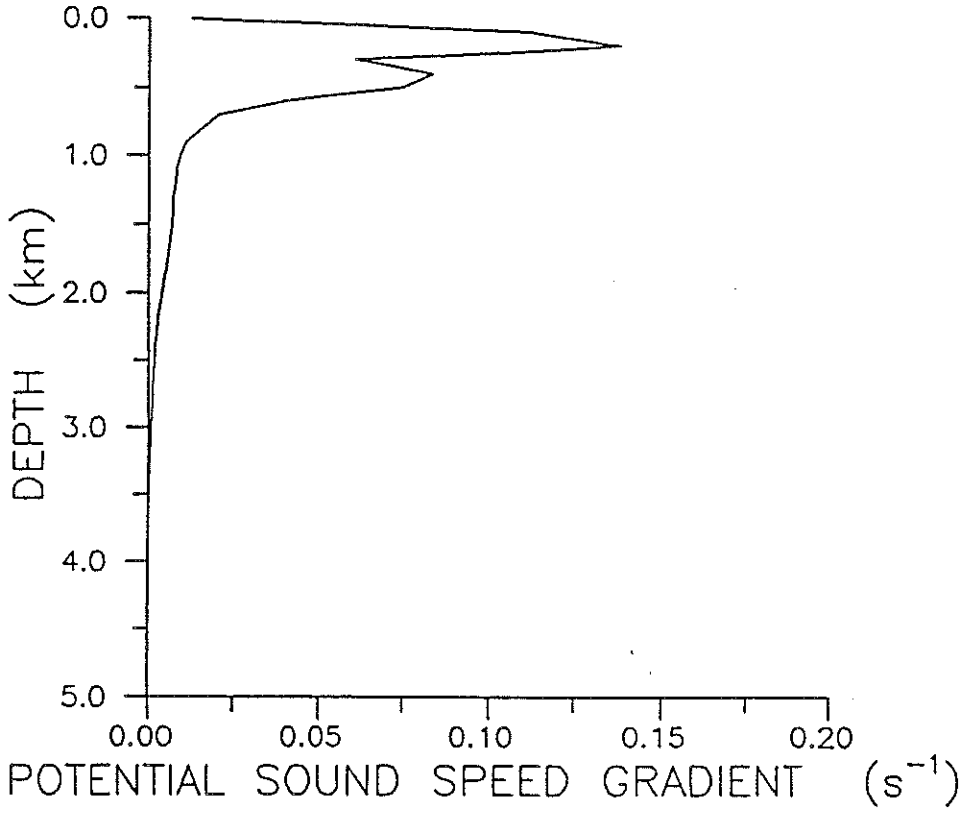

Fig. 2. The climatological potential sound speed gradient in the Northeast Pacific near 30°N, 150°W.

1.3 The Forward Problem for Modes

Miller (1986) demonstrates that the barotropic oscillations in the QG model consist of a summation of resonant Rossby (planetary) basin modes which are excited by the mesoscale turbulence of the free jet region. Solutions for the flat bottom, normal modes are given by,

$$\psi_{nm}(x,y,t) = \mathrm{Re}\Big\{ A_{nm} \exp(i\frac{\beta x}{2\sigma_{nm}}) \sin(\frac{n\pi x}{L}) \sin(\frac{m\pi y}{L}) \exp(i\sigma_{nm} t) \Big\} \quad , \qquad (1.9)$$

where A_{nm} is the amplitude coefficient ($\mathrm{m}^2\ \mathrm{s}^{-1}$), β is the gradient of the Coriolis parameter, L is the length of a side in the square basin, n, m are positive integers and Re{x} denotes

the real part of x (Pedlosky, 1979). The modal frequency is defined as,

$$\sigma_{nm} = \frac{\beta}{\frac{2\pi}{L}\sqrt{n^2+m^2}} \quad .$$

We seek to determine the travel time changes due to the individual modes. The travel time changes due to the pressure and temperature fluctuations associated with these modes are about an order of magnitude smaller than the fluctuations due to currents (Spiesberger et al., 1988a). Equation (1.1) simplifies to,

$$\delta T(t) \cong -\frac{1}{c_0^2}\int_{\Gamma_0} \vec{u}\cdot\hat{s}\ ds \quad , \tag{1.10}$$

where $\vec{u}$ is the current associated with the mode, and the small variation of the sound speed is neglected. The horizontal currents are,

$$\begin{aligned} u(x,y,t) &= -A_{nm}(\frac{m\pi}{L})\cos(\frac{\beta x}{2\sigma_{nm}})\cos(\frac{m\pi y}{L})\sin(\frac{n\pi x}{L})\cos(\sigma_{nm}t) \quad , \\ v(x,y,t) &= A_{nm}\Big\{(\frac{n\pi}{L})\cos(\frac{\beta x}{2\sigma_{nm}})\cos(\frac{n\pi x}{L}) - \\ &\quad (\frac{\beta}{2\sigma_{nm}})\sin(\frac{\beta x}{2\sigma_{nm}})\sin(\frac{n\pi x}{L})\Big\}\sin(\frac{m\pi y}{L})\cos(\sigma_{nm}t) \quad . \end{aligned} \tag{1.11}$$

For a tomographic section oriented along a north-south direction, equations (1.10) and (1.11) yield,

$$\delta T(t) \cong -\frac{Rv(x,y,t)}{c_0^2} \quad , \tag{1.12}$$

where the range between the tomographic instruments is R.

1.4 Selection of Section Location

We want to place the tomographic array in a portion of the QG model that is representative of the Northeast Pacific Ocean because this study is investigating the feasibility

of utilizing a 3000 by 4000 km tomographic array in the Northeast Pacific to search for such modes (Spiesberger et al., 1988a). Using Roden's section of the Pacific along 158°W as a reference, typical eddy-like features (wavelengths of 100 to 200 km) perturb the in-situ sound speed by about 0.2 to 0.5 m s^{-1} at 1000 m depth. This corresponds to vertical displacements between 20 to 50 m (Fig. 3).

A significant problem of this QG model is the inadequate zonal penetration of both the eastward, mid-latitude jet and of the abyssal mean and eddy kinetic energies (Schmitz, 1982). The model's deep gyre extends to 1000–1200 km from the western boundary, whereas Worthington (1976) found that it extends to 2500 km in the North Atlantic. As a result, direct comparisons cannot be made between the model and the ocean at equivalent distances but a scaling factor must be used instead.

The QG sea surface elevation spectra levels are comparable to those of Pacific island stations only in the band between 25–50 days period (Miller, 1986). On either side of this band, the model spectra levels computed at a point just beyond the farthest eastward penetration of the free jet are roughly 10 dB lower than those computed by Luther (1982) for several stations.

The resonant modes within this band usually have longer wavelengths in the north-south direction than in the east-west direction (see Table 1; Miller, 1986). To maximize the response of the acoustic travel times, a north-south section is desirable. We focus our efforts on detecting mode 17, and place a 4000 km length section at x=1160 km where the amplitude of the modal current in the meridional direction has a maximum value. Parameters for this mode are listed in Table 1. At this value of x in the QG model, the interface displacements (at 1000 m depth) are about 5 to 50 m which are comparable to Roden's observations (Fig. 4).

The position of the tomographic section with respect to the mid-latitude jet is shown in Figure 5. Measurements of the sea surface elevation and the meridional current are taken

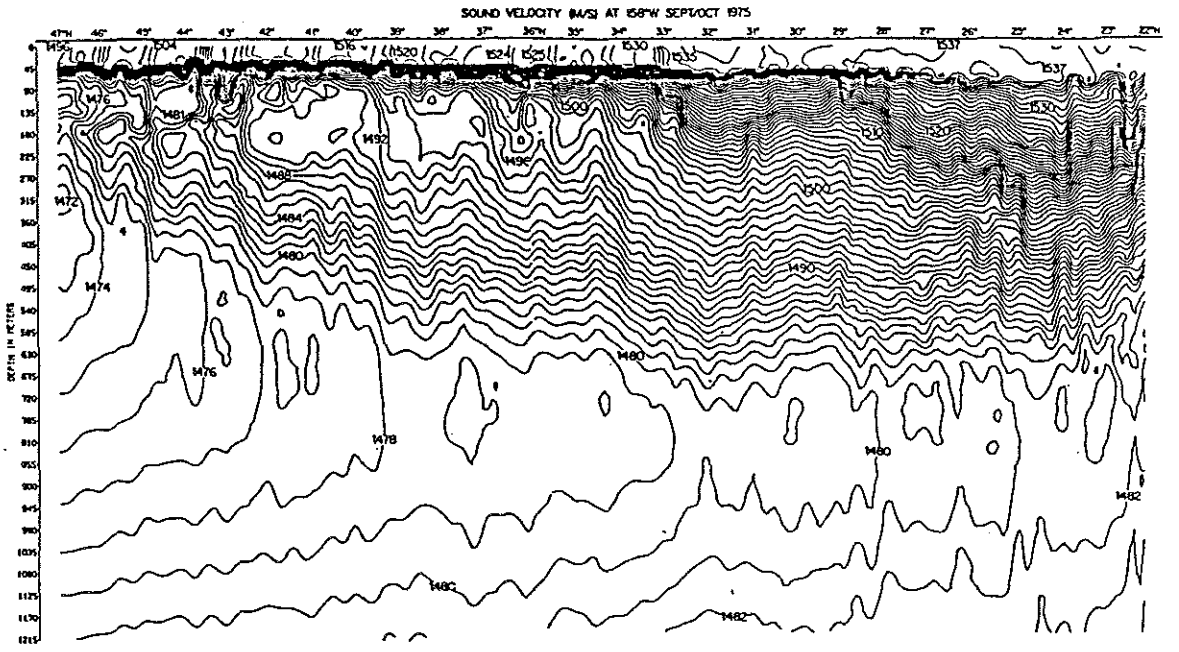

Fig. 3. A meridional section of sound speed in the Northeast Pacific. Contour intervals are at 1 m s^{-1}. We thank Roden for permission to use his figure.

at y=1500 km, and we refer to this location as station 1. The free jet meanders with time and its effects are felt approximately 600 km to either side of the mid-basin point (y=2000 km). On the average, the section is just within the farthest penetration of the jet, the region at which the eddies break off and travel toward the western boundary. Station 1 and the central portion of the tomographic section are influenced by eddy processes.

In summary, it is difficult to locate a region of this model whose eddy field is similar to that found in the Northeast Pacific. However, we believe that the selected section is realistic enough so that a comparison of the tomographic and point measurements provides a useful guide for further investigation.

(n,m)	Period (days)	λ_x (km)	λ_y (km)	rms Amp. (cm)	rms Vel. (cm s^{-1})
5,1	29.1	1600	8000	1.1	0.7

Table 1. The scales of mode 17 in this QG model. The x and y wavelengths are indicated along with the rms values of the maximum sea surface displacement and the maximum meridional current.

1.5 Spectral Analysis

Four years of statistically steady state streamfunction values are sampled at 4-day intervals. Three acoustic travel time series are generated from three acoustic rays traveling between a source and a receiver. The source and receiver are at depths of 800 m and are separated by 4000 km (Fig. 5). The angles of the rays at the source (with respect to the horizontal) are 11.7°, 6.3° and 2.1°, and their upper turning depths are 154 m, 447 m and 638 m, respectively. The rays are traced through a climatological sound speed profile in the Northeast Pacific at the same location at which the potential sound speed gradient is computed (Fig. 2). The travel time series for the 11.7° ray is detrended by a smoothed cubic spline so that periods greater than about one year are removed (Fig. 6). Time series are recorded for sea surface elevation along with upper and lower layer meridional currents for comparison against the series of detrended travel time change for the 11.7° ray (Fig. 7). The fluctuations of sea level and meridional current have a predominant period of 40–45 days. A dominant period is not visually evident in the travel time fluctuations.

The power spectral density levels are computed by dividing each time series into 4 non-overlapping segments, each of which has a duration of approximately one year. A Bartlett window is applied to the data, so the spectral estimates are Chi-squared random variables with 12 degrees of freedom (Jenkins and Watts, 1968). The highest sidelobe level for this window is -25 dB (Oppenheim and Schafer, 1975).

Within the band of interest (25–50 days), the sea level and current spectra are similar

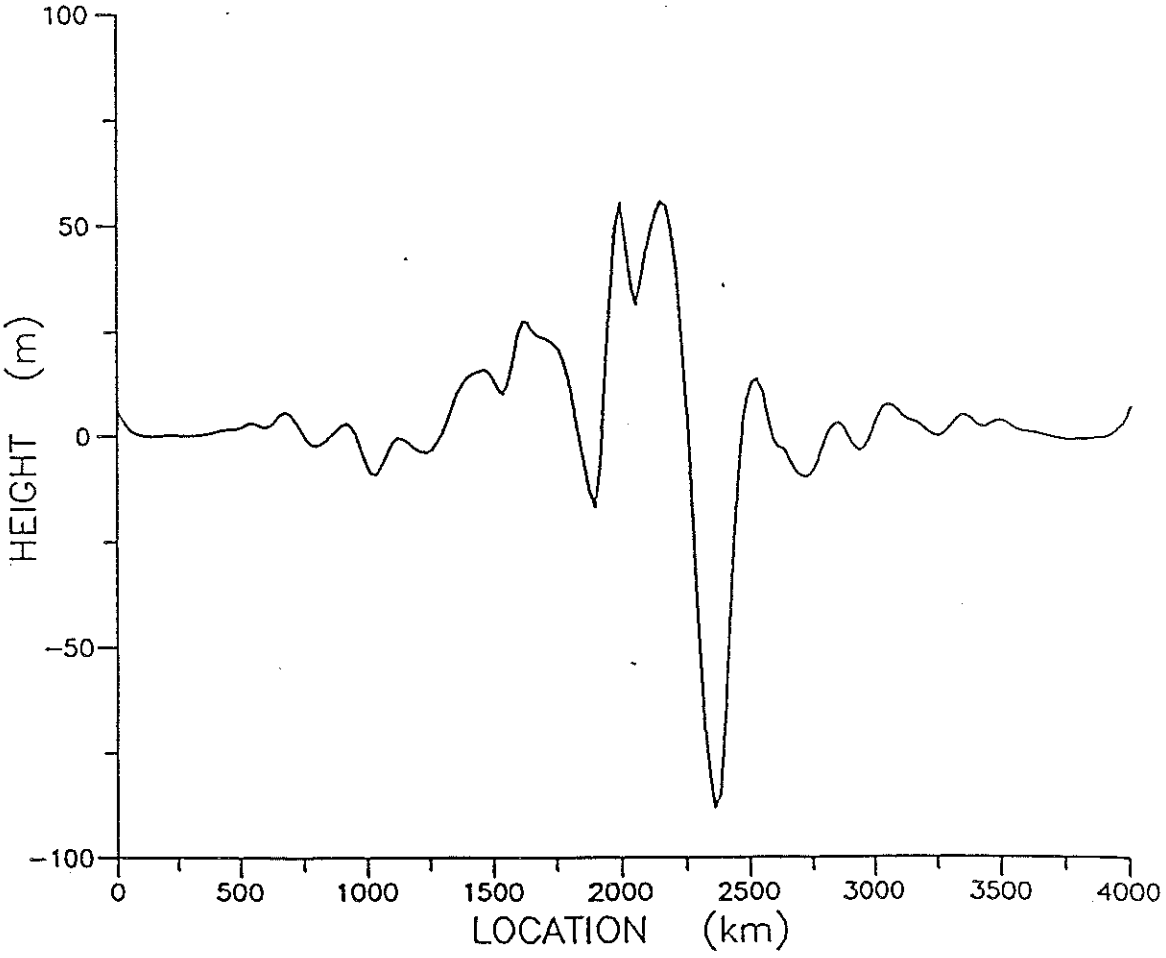

Fig. 4. Perturbation interface displacement of the 2-layer QG model on day 4. The large-scale features in the middle of the section are due to the mid-latitude free jet.

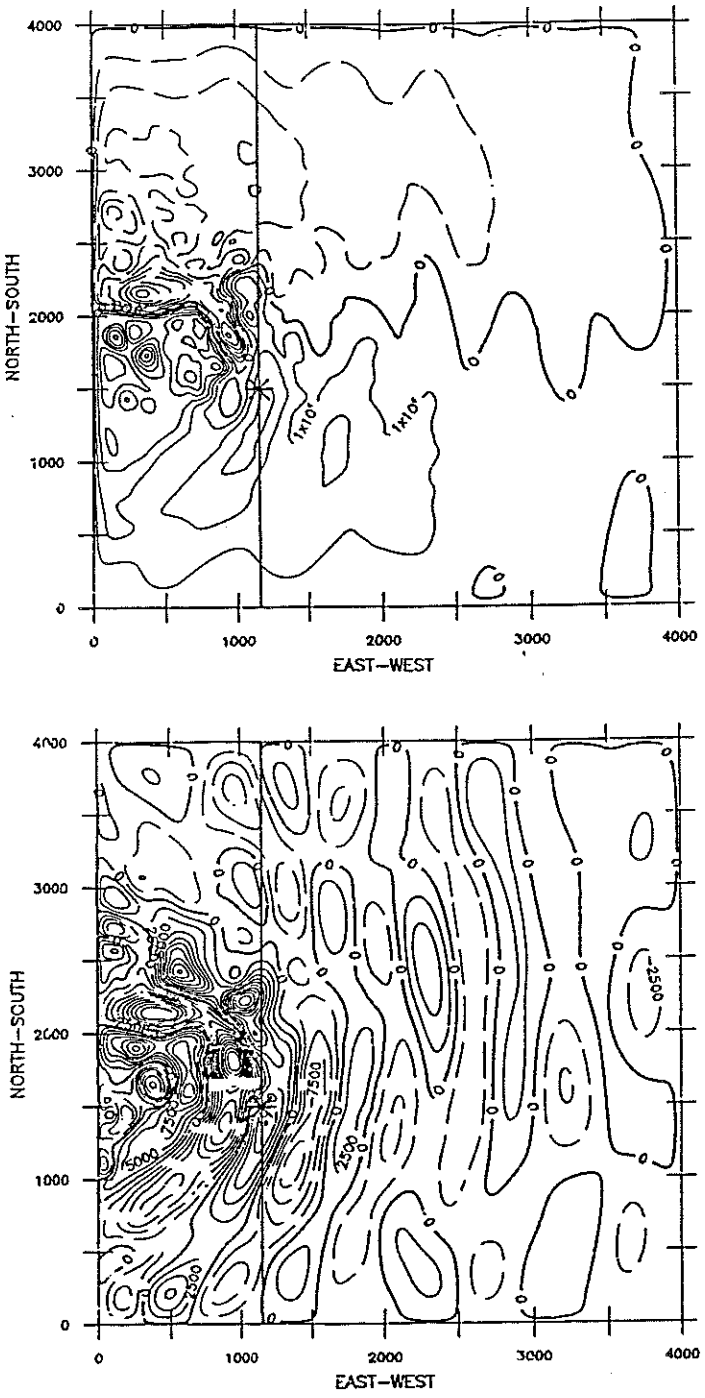

Fig. 5. Upper: Map of the upper layer streamfunction on day 4. The solid line indicates the position of the tomographic section (x=1160 km) and the asterisk marks the location of station 1 where the sea surface elevation and currents are computed (y=1500 km). Contour interval is 1×10^4 m^2 s^{-1} and the dashed lines correspond to negative values. Bottom: Same except for the lower layer. The contour interval is 0.25×10^4 m^2 s^{-1}.

in shape (Fig. 8). The three spectra exhibit a broad peak centered near .025 cpd (40 day period), and are similar to Miller's results (see his Figures 3b, 4e and 5e). The spectrum of the travel time change for the 11.7° ray also displays a broadband peak in the same band along with a peak at a period of 28.6 days which is significant at the 95% confidence level (Fig. 8). This peak is also significant at the 95% level in the spectra of the other two rays (not shown).

Is this peak caused by mode 17? We tentatively identify the peak as mode 17 which has a theoretical period of 29.1 days. Using equation (1.12), we calculate the travel time change due to this mode. If we assume the modal energy is spread uniformly in a bandwidth Δf (cpd), the power spectral density level P_o (s^2 cpd^{-1}) is given by,

$$P_o = \frac{\sigma_{\delta t}^2}{\Delta f} \quad ,$$

where $\sigma_{\delta t}^2$ is the variance of the travel time fluctuation caused by the mode. Table 2 lists the predicted and measured rms travel time change and spectral level for this mode. The predicted spectral level of 3.18×10^{-2} (s^2 cpd^{-1}) is computed using a half-power bandwidth of .002 cpd which is a Q of about 17 (Miller, 1986). The observed spectral level of this peak is about 1.69×10^{-2} (s^2 cpd^{-1}). The predicted and observed levels are similar.

We seek to determine the influence of the eddy field on the travel times to ensure that the peak is not the result of mesoscale processes. The QG model is high-passed filtered using a Bartlett window. For this filter, wavelengths of 800, 1000 and 2000 km are attenuated by -3.4, -6.1 and -16.0 dB, respectively. Therefore, the mesoscale field is passed and the long-scale planetary modes are attenuated. The averaged periodogram of the travel times is computed over the four-year record for the high-passed model (Fig. 9). The spectral level is about 30 dB less than the peak at 28.6 days observed in the unfiltered model. Therefore we conclude that the peak at a period of 28.6 days is caused by a planetary basin mode rather than the mesoscale field.

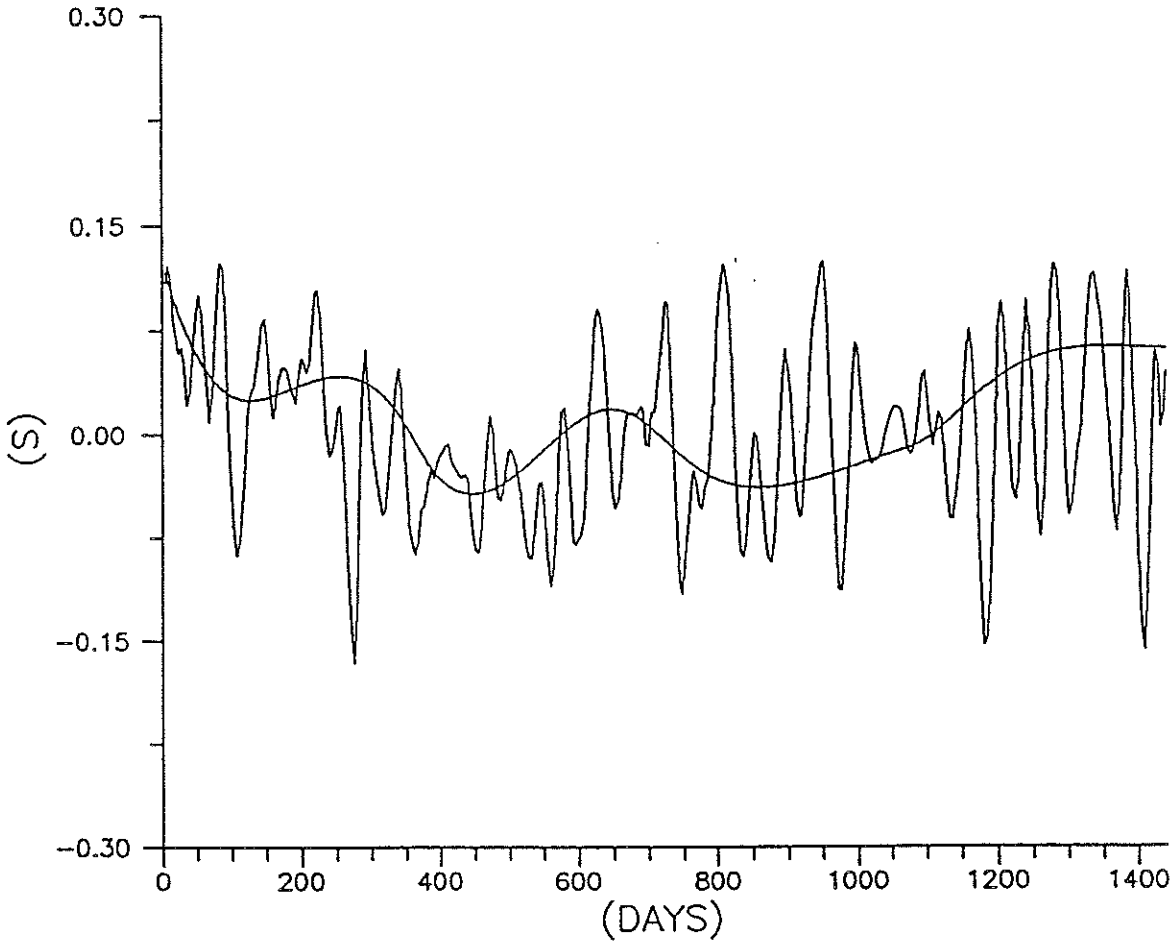

Fig. 6. The entire time series of acoustic travel time change for the 11.7° ray overlaid by the smoothed cubic spline which is used to detrend it.

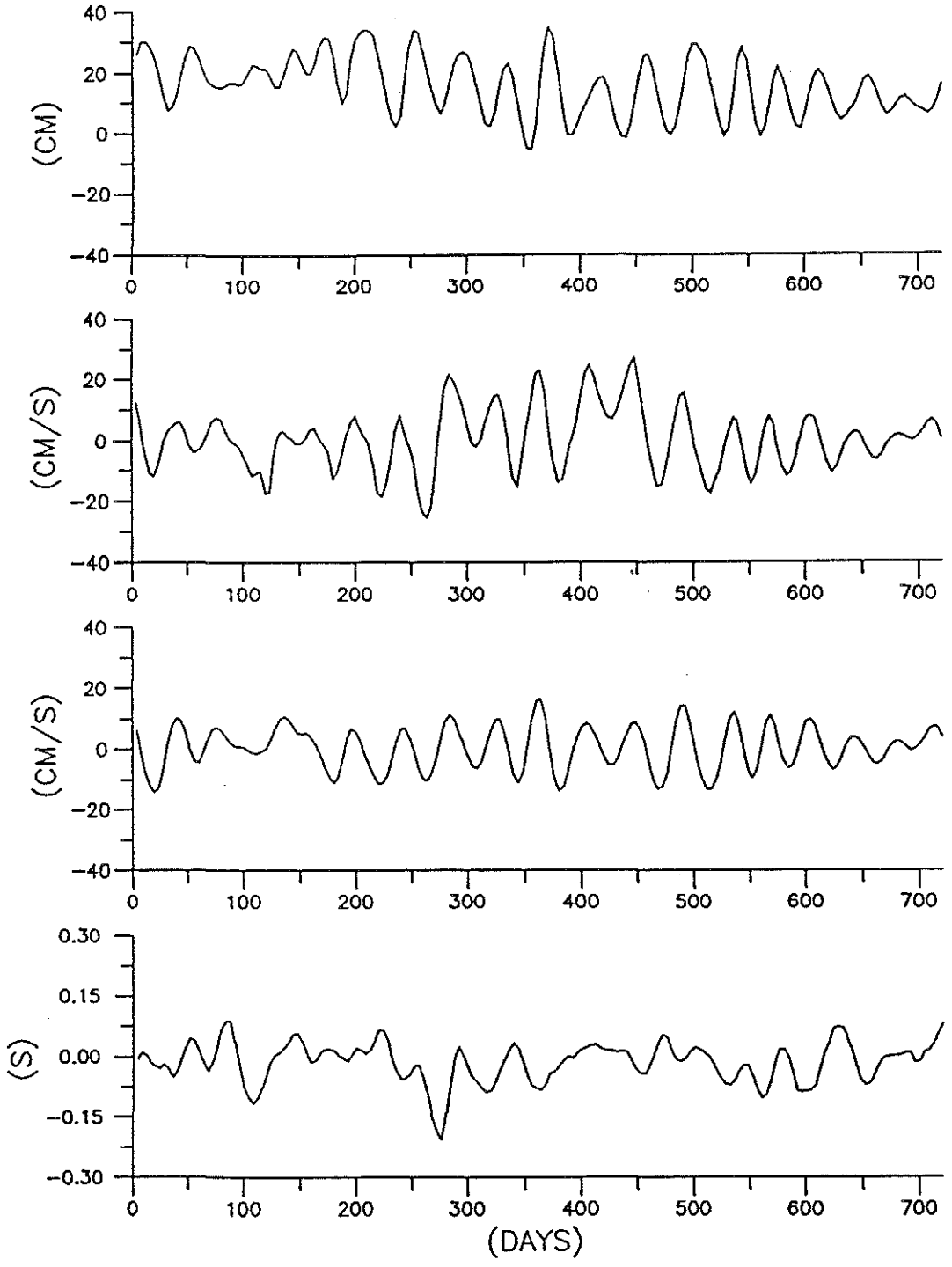

Fig. 7. Time series of sea surface elevation, upper layer meridional current, lower layer meridional current and detrended acoustic travel time change for the 11.7° ray (from top to bottom). Elevation and current are measured at x=1160 km, y=1500 km (Fig. 5). The first 2 years of the 4-year records are displayed. The values are computed at 4-day intervals.

	rms Travel Time Change (ms)	Spectral Level (s^2 cpd^{-1})
Predicted	−11.27	3.18×10^{-2}
Measured	7.82	1.69×10^{-2}

Table 2. The predicted values of the rms travel time change and the power spectral density level are compared with the values computed from the tomographic array. The predicted rms travel time change is obtained from eqn. (1.12).

1.6 Discussion

Although basin-scale resonant barotropic modes have been detected in numerical models (for example Willebrand et al., 1980; Miller, 1986), attempts to detect this type of motion in the real ocean have not been as successful. Luther (1982) presented the most convincing but, by his own admission, still inconclusive evidence of a barotropic vorticity mode from his analysis of sea level records covering a wide geographic area in the Pacific.

Luther (1983) gives two reasons for the lack of direct observations of basin-scale vorticity modes in the ocean. First, because the modes are weakly excited, their signal may not be strong enough relative to the background noise to be extracted from the data he used. Second, topography reduces the period and scale of a planetary mode, changing it into a topographic mode that is restricted to the vicinity of the controlling feature.

In this QG model, two factors hinder the observations of barotropic planetary modes in the sea surface and current records. First, the mesoscale field masks the signals of the modes in the point measurements. Second, because the modes are closely spaced in frequency, the presence of friction and non-linearities can cause the narrow modal peaks to broaden into a broadband peak (Miller, 1986). However, the tomographic system is not as strongly affected by these factors. A basin-scale tomographic array attenuates the signals from the mesoscale processes so that a mode near 28.6 days can be detected at the 95% confidence limit for a

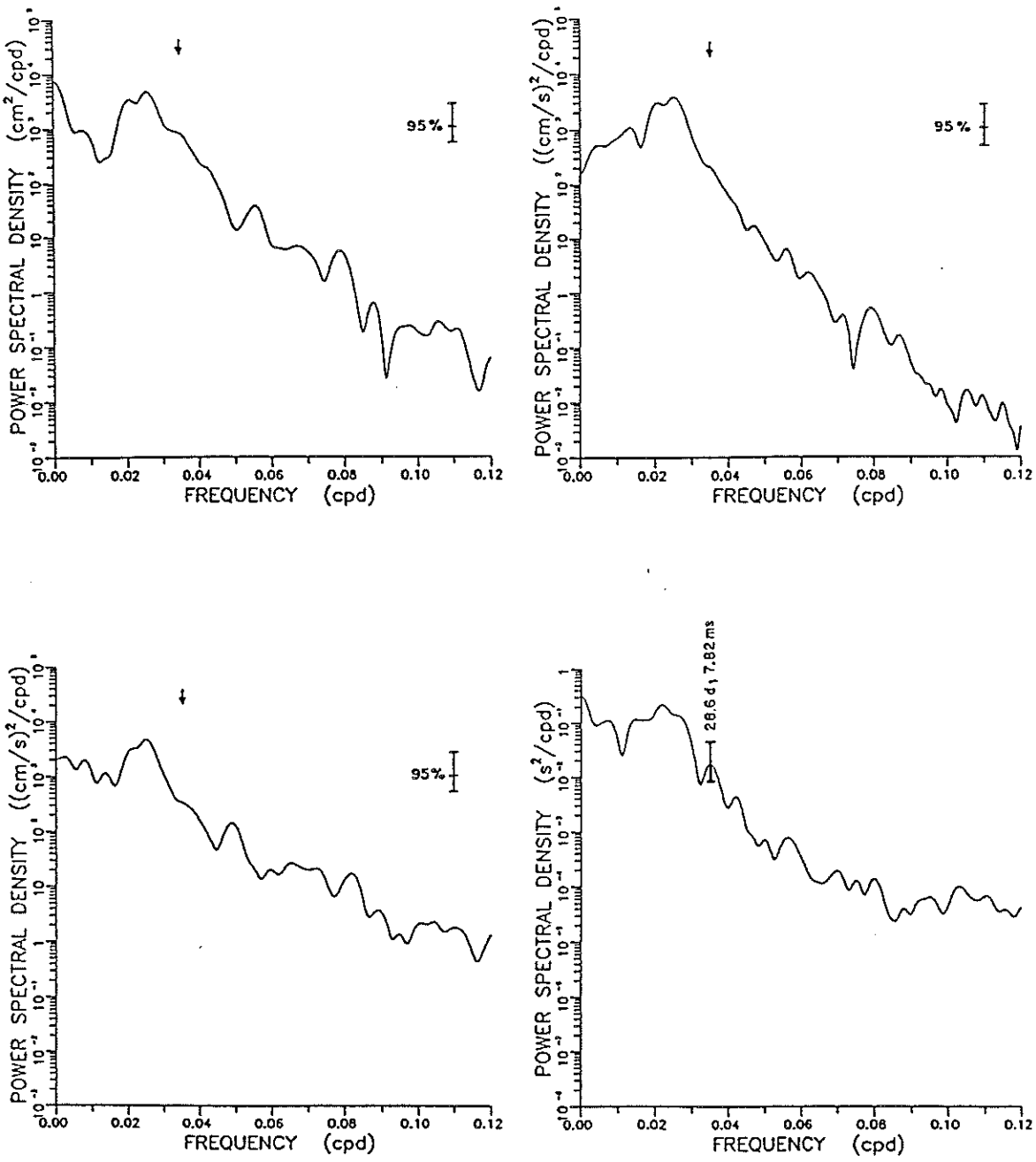

Fig. 8. Power spectral densities of sea surface displacement (upper left) and meridional currents in the upper and lower layers (lower left and upper right) at station 1 and acoustic travel time change for the 11.7° ray (lower right) computed over the 4-year record. In the travel time figure, the period and rms travel time of mode 17 are labeled. In the other figures, the arrow marks the period of the mode. The 95% confidence limits are shown.

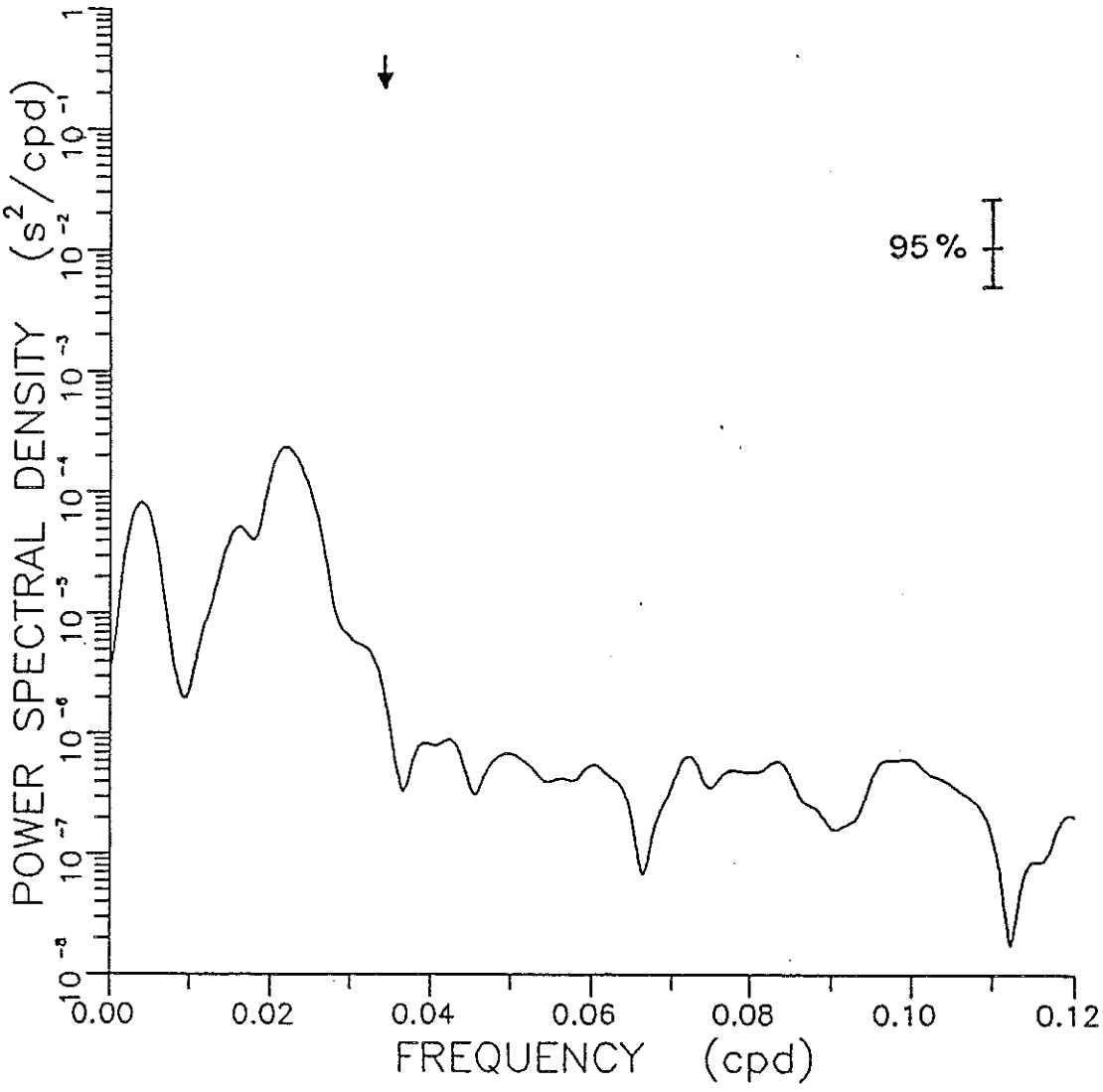

Fig. 9. The power spectral density of acoustic travel time change for the 11.7° ray traveling through the eddy field (but not the large-scale field). The arrow marks the period of mode 17, and the 95% confidence limit is shown.

record length of four years. In other words, the acoustic travel time changes are given by a spatial integral between the source and the receiver which preferentially attenuates the short wavelengths in the ocean (Spiesberger et al., 1988a). Also, the tomographic measurements are able to resolve an individual mode by placing the section at a position where the modal current has a maximum value.

Spiesberger et al., (1988a,b) have demonstrated that the acoustic phase of the tomographic signals might be used to make estimates of relatively slow barotropic currents whose length scales are large (order of 1000 km or more). No one knows what the spectra of acoustic travel times over basin-scale distances look like for periods greater than a few days. However, the internal wave field imposes a limit. For a tomographic array consisting of one source and ten receivers at about 4000 km range, the threshold at which a basin-scale current can be detected with a confidence of 95% is given by $u \cong 33.6T$ micro-meters per second where the period of the oscillation, T, is expressed in days. For mode 17, T is approximately 29 days, and the threshold speed is 0.1 cm s^{-1}. The amplitude of the mode 17 current in this QG model is 1.0 cm s^{-1}. Therefore, if internal waves limit the precision of the tomographic array and the real ocean contains modes whose scales are similar to those in the QG model, then the modes would be detected by the tomographic system.

Platzman (1981) has computed the periods of the ocean's modes for the range between 8 and 80 hours. Any experimental program which searches for modes with periods exceeding 80 hours would be greatly enhanced by an extension of the numerical calculations to longer periods. However, at these longer periods, the stratification of the ocean and the non-linear interaction of the modes with other large-scale currents near the same period may be important both for the interpretation of the data and for a reliable numerical computation of the modal structure.

References

Bushong, P.J., 1987: Tomographic Measurements of Barotropic Motions. Masters Thesis, Joint Program in Oceanography, Massachusetts Institute of Technology and the Woods Hole Oceanographic Institution, 48pp.

Chiu, C.S. and Y. Desaubies, 1987: A Planetary Wave Analysis Using the Acoustic and Conventional Arrays in the 1981 Ocean Tomography Experiment. *J. Phys. Ocean.*, **17**, 1270–1287.

Gill, A.E., 1982: Atmosphere-Ocean Dynamics. Academic Press Inc., New York, 662pp.

Haidvogel, D.B. and W.R. Holland, 1978: The Stability of Ocean Currents in Eddy-Resolving General Circulation Models. *J. Phys. Ocean.*, **8**, 393–413.

Holland, W.R., 1978: The Role of Mesoscale Eddies in the General Circulation of the Ocean—Numerical Experiments Using a Wind-Driven Quasi-Geostrophic Model. *J. Phys. Ocean.*, **8**, 363–392.

— and W.J. Schmitz, 1985: Zonal Penetration Scale of Model Midlatitude Jets. *J. Phys. Ocean.*, **15**, 1859–1875.

Howe, B.R., P.J. Worcester and R.C. Spindel, 1987: Ocean Acoustic Tomography: Mesoscale Velocity. *J. Geophys. Res.*, **92**, 3785–3805.

Jenkins, G.M. and D.G. Watts, 1968: Spectral Analysis and its Applications. Holden-Day Inc., Oakland, 525pp.

Luther, D.S., 1982: Evidence of a 4–6 Day Barotropic, Planetary Oscillation of the Pacific Ocean. *J. Phys. Ocean.*, **12**, 644–657.

—, 1983: Why Haven't You Seen an Ocean Mode Lately. *Ocean Modelling*, **50**, 1–6.

Malanotte-Rizzoli, P. and W.R. Holland, 1985: Gyre-Scale Acoustic Tomography: Modeling Simulations. *J. Phys. Ocean.*, **15**, 416–438.

Marple, S.L., 1983: Digital Spectral Analysis with Applications. Prentice-Hall, Inc., Englewood Cliffs, 492pp.

Miller, A.J., 1986: Barotropic Planetary-Topographic Oscillations in Ocean Basins. Ph.D dissertation, University of California San Diego, 133pp.

—, 1987: Open-Ocean Response and Normal Mode Excitation in an Eddy-Resolving General Circulation Model. *Geophys. and Astrophys. Fluid Dynamics*, **37**, 253–278.

Munk, W.H., 1974: Sound Channel in an Exponentially Stratified Ocean, with Application to SOFAR. *J. Acoust. Soc. Am.*, **55**, 220–226.

—, P.J. Worcester and F. Zachariasen, 1981: Scattering of Sound by Internal Wave Currents: The Relation to Vertical Momentum Flux. *J. Phys. Ocean.*, **11**, 442–454.

Oppenheim, A.V. and R.W. Schafer, 1975: Digital Signal Processing. Prentice-Hall, Inc., Englewood Cliffs, 585pp.

— and A.S. Willsky, 1983: Signals and Systems. Prentice-Hall, Inc., Englewood Cliffs, 796pp.

Pedlosky, J., 1979: Geophysical Fluid Dynamics. Springer-Verlag, New York, 624pp.

Platzman, G.W., 1975: Normal Modes of the Atlantic and Indian Oceans. *J. Phys. Ocean.*, **5**, 201–221.

—, G.A. Curtis, K.S. Hansen and R.D. Slater, 1981: Normal Modes of the World Ocean. Part II: Description of Modes in the Period Range 8 to 80 Hours. *J. Phys. Ocean.*, **11**, 579–603.

Roden, G.I., 1984: Mesoscale Sound Speed Fronts in the Central and North Pacific. *J. Phys. Ocean.*, **14**, 1659–1669.

Schmitz, W.J. and W.R. Holland, 1982: A Preliminary Comparison of Selected Numerical Eddy-Resolving General Circulation Experiments with Observations. *J. Mar. Res.*, **40**, 75–117.

Spiesberger, J.L., P.J. Bushong, K. Metzger and T.G. Birdsall, 1988a: Basin-Scale Tomography: Synoptic Measurements of a 4000 km Length Section in the Pacific between the Periods of 4 Minutes and 34 Hours Using Acoustic Phase. Submitted to *J. Phys. Ocean.*.

—, P.J. Bushong, K. Metzger and T.G. Birdsall, 1988b: Estimating the Acoustic Travel Time over a 4000 km Length Section of the Pacific Using the Phase of Pulse-Like Signals. Submitted to *IEEE, J. Ocean Eng.*.

Willebrand, J., S.G.H. Philander and R.C. Pacanowski, 1985: The Oceanic Response to Large-Scale Atmospheric Disturbances. *J. Phys. Ocean.*, **10**, 411–429.

Worthington, L.V., 1976: On the North Atlantic Circulation. The Johns Hopkins Oceanographic Studies, **6**, 110pp.